Failure of Compression-Loaded Multidirectional Composite Laminates

Mark J. Shuart*
NASA Langley Research Center, Hampton, Virginia

An analytical and experimental investigation of the failure of selected compression-loaded $[\pm\theta/\mp\theta]_{6s}$ composite laminates is described. A general nonlinear theory is presented for predicting a laminate's compressive strength and failure mode. The theory includes the effects of out-of-plane ply waviness, in-plane fiber waviness, and fiber scissoring. A simple compressive test technique is used to obtain the experimental data. The analytical and experimental results show good agreement for $\theta < 45$ deg and show excellent agreement for $\theta \geq 45$ deg. The dominant compression failure modes for the laminates in this study were found to be interlaminar shearing, in-plane matrix shearing, and matrix compression.

Introduction

EFFICIENT designs using composite materials require a thorough understanding of the mechanisms that affect laminate response. Laminate compressive strength is an important design parameter, and researchers have studied the mechanics of this phenomenon for many years. Dow and Gruntfest[1] postulated that the compressive failure of unidirectional laminates was the result of the fibers buckling within the matrix. Rosen[2] developed a model for unidirectional laminates that focused on fiber instability and predicted the compressive strength of such laminates. Greszczuk[3,4] studied the effects of the constituents on the compressive strength of fiber- and lamina-reinforced composite materials. These studies focused on unidirectional laminates. Several researchers[5-8] have conducted detailed studies of the fiber kinking failure mechanism for compression-loaded unidirectional laminates. Suarez et al.[9] studied failure due to outer-ply instability for compression-loaded multidirectional laminates. Some of their experimental results agreed with predicted strengths when the initial waviness of the outer plies was included in the analysis. Rotem and Hashin[10] and Kim[11] conducted experimental studies of the failure of angle-ply laminates. These studies showed that shearing failure mechanisms significantly affected the failure of angle-ply laminates. A nonlinear theory was proposed in Ref. 12 for predicting the strength of compression-loaded multidirectional laminates. The initial waviness of all plies was included in the theory, and two shearing mechanisms that initiate failure were analyzed: interlaminar shearing caused by initial waviness of the plies and in-plane matrix shearing. The compressive strength of $[\pm\theta]_s$-class laminates for $0 \leq \theta \leq 75$ deg was predicted by the theory in Ref. 12. A general, validated theory that quantifies the dominant mechanisms affecting the compressive strength of multidirectional composite laminates ($0 \leq \theta \leq 90$ deg) would be useful for understanding laminate strength.

The current investigation was conducted to study the failure of selected compression-loaded multidirectional composite laminates. A general nonlinear theory is described that quantifies the dominant mechanisms affecting the compressive strength for a wide range of undamaged composite laminates. This theory is an improvement of the theory in Ref. 12. A matrix compression failure mode is included in the improved theory, and the in-plane matrix shearing mechanism is generalized to include effects from in-plane fiber waviness and from fiber scissoring. Experimental results are also presented for graphite-epoxy specimens. The specimens were tested using a simple compressive test technique. The experimental results include compressive strength data and descriptions of laminate failure modes. These experimental results are compared with predicted results.

Analysis

The geometry of a typical laminate is illustrated in Fig. 1. The laminate has length a and width b. A $+\theta$ fiber orientation is indicated in the figure. The laminate is symmetric with respect to the middle surface, which is $z = 0$ plane.

Two types of initial imperfections for composite laminates are shown in Fig. 2. Out-of-plane waviness or ply waviness is shown in Fig. 2a, and in-plane waviness or fiber waviness is shown in Fig. 2b. These initial imperfections are typical for composite laminates and may be the result of residual thermal stresses. Initial imperfections similar to those shown in Fig. 2 can affect the response and failure of composite laminates, and these imperfections are modeled in the present study. All calculations use an imperfection-amplitude-to-ply-thickness ratio of 0.5. A nominal ply thickness is 0.13 mm.

The analysis used in this study is presented in this section. The theory from Ref. 12 is the foundation for the present analysis and is summarized. Improvements to the theory in Ref. 12 are described. The criteria for predicting laminate failure are also summarized.

Background

The nonlinear theory in Ref. 12 models a ply as a plate supported by a linear elastic foundation. Kirchhoff plate the-

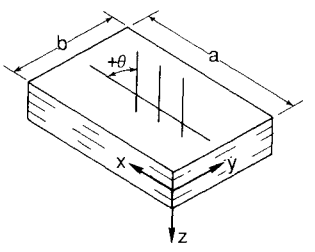

Fig. 1 Coordinate system and dimensions for a typical laminate.

Received July 5, 1988; revision received Dec. 23, 1988.

*Aerospace Engineer, Structural Mechanics Branch. Senior Member AIAA.

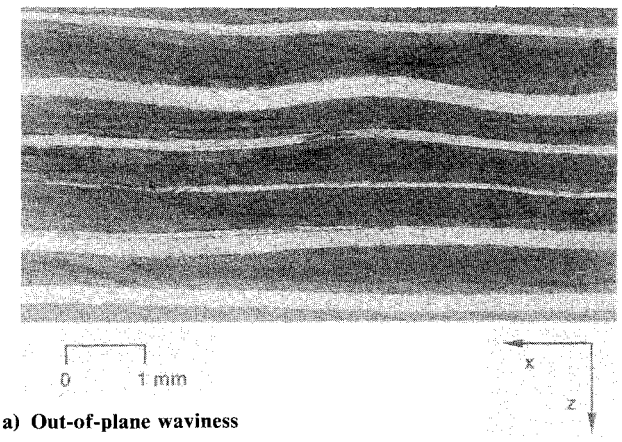

a) Out-of-plane waviness

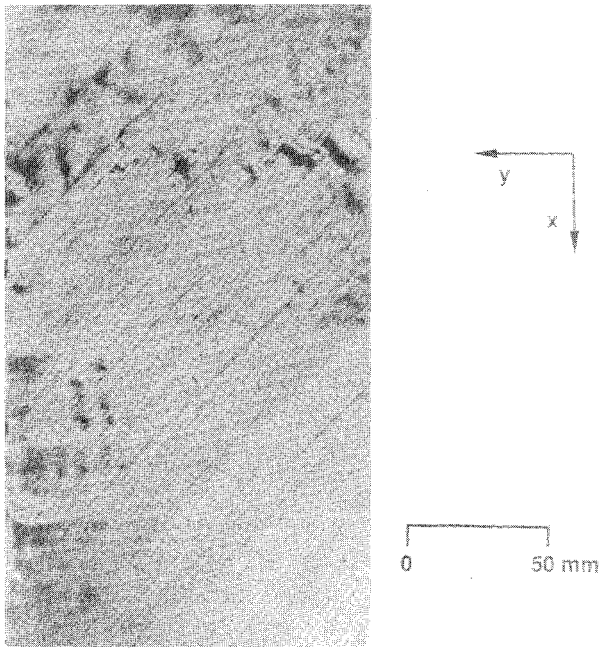

b) In-plane waviness

Fig. 2 Initial imperfections in composite laminates.

Table 1 Typical material properties

Graphite-epoxy:	
Longitudinal Young's modulus, E_{11}; GPa	127.6
Transverse Young's modulus, E_{22}; GPa	11.3
Shear modulus, G_{12}; GPa	6.0
Major Poisson's ratio, ν_{12}	0.30
Neat resin[13]:	
Young's modulus, E_m; GPa	3.7
Shear modulus, G_m; GPa	1.8
Major Poisson's ratio, ν_m	0.36

ory and von Kármán strain-displacement relations are used for the plate, and these relations include contributions from out-of-plane initial imperfections. The plate properties are typical linear elastic properties for a graphite-epoxy ply. Foundation deformations are expressed as functions of the displacements for the adjacent plates. The foundation properties are linear elastic neat resin properties.[13] The plate and foundation material properties are summarized in Table 1.

The theory in Ref. 12 models a laminate as a series of plates and elastic foundations. Each plate has an out-of-plane initial imperfection that is the same shape as the critical short-wavelength buckling mode shape for the laminate.[14] Short-wavelength buckling is characterized by a mode shape whose half-wavelength is much smaller than the laminate's length or width. The initial imperfection w_0 is expressed as

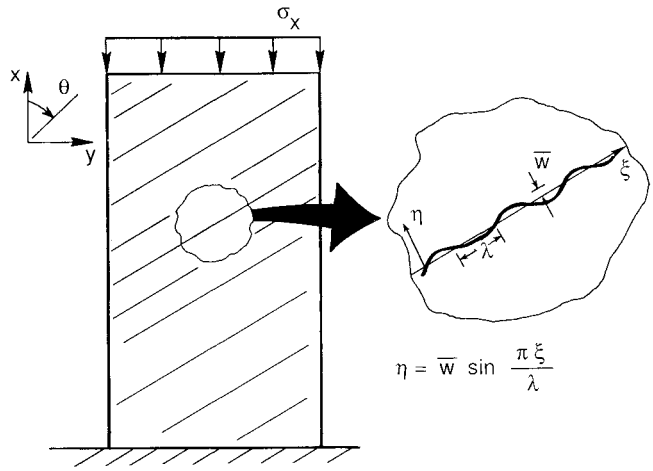

Fig. 3 Idealized in-plane waviness for $[\pm\theta]_s$-class laminates.

$$w_0 = \bar{w}_0 \sin(\pi y/b) \sin(\pi x/\lambda) \tag{1}$$

where $\bar{w}_0$ is the amplitude of the initial imperfection and λ the half-wavelength for the critical short-wavelength buckling mode shape. The calculation of λ is described in Ref. 12. The laminate is loaded in the x direction by a uniform end shortening. Nonlinear equilibrium equations for each laminate are derived using the principle of stationary potential energy. The nonlinear equations are used to obtain displacements, strains, loads, and stresses for the laminate.

Response Mechanisms for Compression-Loaded Laminates

The present theory is used to predict three failure modes for compression-loaded composite laminates: interlaminar shearing, in-plane matrix shearing, and matrix compression. The interlaminar stresses investigated in the present study are caused by the geometrically nonlinear behavior of the plies and are different from the interlaminar stresses at a free edge that are caused by ply material property differences. Ply waviness causes the interlaminar stresses discussed in the present study, and these stresses lead to the interlaminar shearing failure mode. The in-plane matrix shearing failure mode occurs in angle plies at the fiber-matrix interface and/or in the epoxy matrix between fibers.[15] In-plane shear stresses parallel to the fiber-matrix interface cause this failure mode. These shear stresses may be a function of both fiber waviness and fiber scissoring. The theory in Ref. 12 does not account for fiber waviness or fiber scissoring. Matrix compression failure is similar to the classic compression failure for isotropic materials wherein the failure surface extends through the material thickness and is oriented at 45 deg to the middle surface. This failure mode may occur in composite laminates when the epoxy matrix is the dominant load-carrying constituent. The matrix compression failure mode is not considered in Ref. 12.

Fiber Waviness

The model used for fiber waviness is illustrated in Fig. 3. The wavy shape of a fiber in a $+\theta$ angle ply is idealized as a sine function having amplitude $\bar{w}$ and half-wavelength λ. This shape is expressed as

$$\eta = \bar{w} \sin(\pi\xi/\lambda) \tag{2}$$

where η is the fiber shape and ξ a coordinate parallel to a $+\theta$ axis. A wavy fiber is globally oriented at θ but also has local perturbations about that angle. The change in fiber angle $\Delta\theta$ along the ξ axis can be expressed as

$$\Delta\theta = \tan^{-1}\left(\frac{d\eta}{d\xi}\right) \tag{3}$$

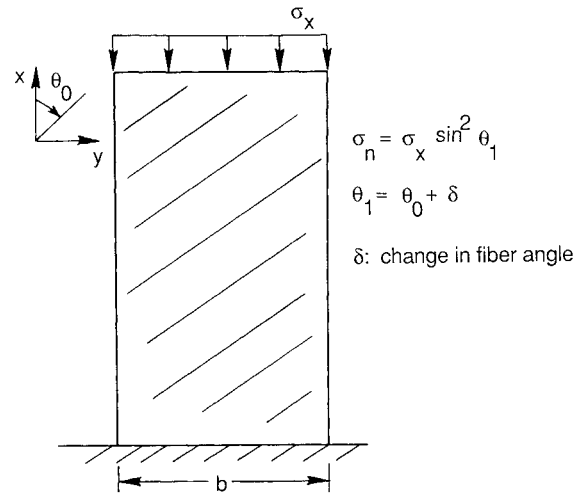

a) Compression-loaded laminate

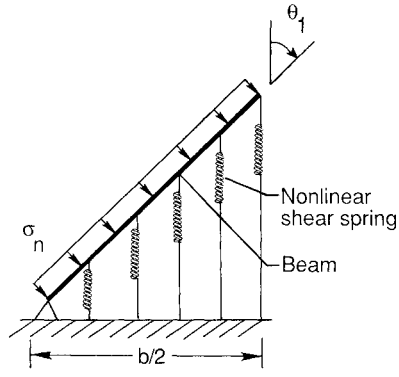

b) Model

Fig. 4 Fiber-scissoring model for $[\pm\theta]_s$-class laminates.

The in-plane shear-stress distribution along the fiber is calculated using classical laminated plate theory as a function of the applied load, the global angle $+\theta$, and the local perturbation $\Delta\theta$. The analysis indicates that the in-plane shear stress at some locations along a $+\theta$ wavy fiber is greater than the in-plane shear stress along a straight $+\theta$ fiber. A failure criterion that uses this shear stress but neglects fiber waviness could give nonconservative results. The amplitude $\bar{w}$ and half-wavelength λ are obtained using the theory in Ref. 12. The present theory assumes that the axial-load-$\bar{w}$ behavior for a wavy fiber is the same as the applied-load-$\bar{w}$ behavior for a $[0_2]_s$ laminate (see Fig. 3.19 of Ref. 12).

Fiber Scissoring

The model used for fiber scissoring is illustrated in Fig. 4. Fiber scissoring in a $+\theta$ angle ply is idealized as a simply supported beam on a nonlinear foundation. The foundation has only shear stiffness, and this stiffness is obtained from the material system's shear-stress/shear-strain behavior. Typical shear-stress/shear-strain behavior in the principal material coordinate system (i.e., parallel and perpendicular to a ply's fiber direction) for AS4/3502 is shown in Fig. 5. The data in the figure were obtained using a $[\pm 45/\mp 45]_{6s}$ laminate and the procedure described in Ref. 16. The tangent shear modulus for a given shear stress is used for the foundation stiffness.

The response of the fiber-scissoring model is governed by a nonlinear equation. The equation is derived from force equilibrium and is expressed as

$$\sigma_x \sin^2\theta_1 - G_{12}(\theta_1 - \theta_0) = 0 \qquad (4)$$

where θ_0 is the initial fiber angle, θ_1 the final fiber angle, σ_x the far-field stress on the laminate, and G_{12} the tangent shear modulus for the material system (i.e., foundation stiffness). The difference between θ_0 and θ_1 is defined as δ. Equation (4) is used to determine the final fiber angle for the given far-field stress on the laminate and for the foundation stiffness. The first term in Eq. (4) corresponds to the applied loading on the beam, and the second term corresponds to the foundation's deformation due to the applied loading. The ply in-plane shear stress in the principal material coordinate system is calculated using the far-field stress on the laminate and classical laminated plate theory. The foundation stiffness is the tangent shear modulus for that shear stress. The far-field stress on the laminate is increased incrementally, and the fiber angle and the in-plane shear stress are calculated.

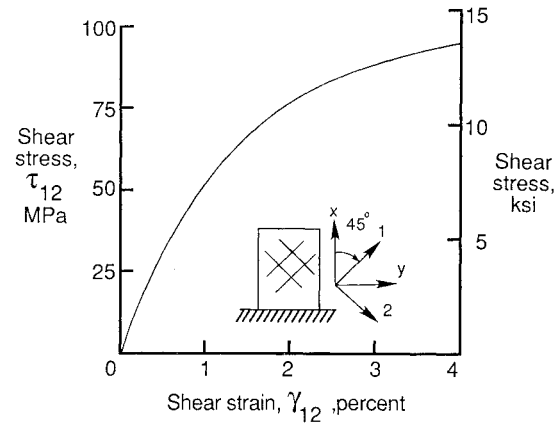

Fig. 5 Shear-stress/shear-strain response for AS4/3502 using a $[\pm 45/\mp 45]_{6s}$ laminate.

Failure Criteria

The results of the present analysis are applied to predict the failure of compression-loaded $[\pm\theta]_s$-class laminates. Specifically, laminate failure is assumed to be initiated by interlaminar shear strains, by in-plane shear stresses, or by matrix compression stresses. The analysis does not couple the failure mechanisms. Interlaminar shearing for a laminate occurs in the foundation between plates and is limited by matrix shearing failure. The shear strain for matrix failure is used for the maximum interlaminar shear strain for the laminate, and this value is 0.036 mm/mm.[13] In-plane shearing for a laminate occurs in the plates and is limited by a ply shearing failure. The shear stress in the principal material coordinate system is used for the maximum in-plane shear stress for the laminate, and this value is 95.1 MPa.[15] The in-plane shearing stresses are used instead of the in-plane shearing strains because such strains are extremely difficult to determine accurately. The difficulty arises from the near-zero slope for the stress-strain response near failure.[15] Matrix compression stresses become significant when the matrix is the principal load-carrying constituent of the laminate. The matrix compression failure mode can occur in $[90]_{48}$ laminates and in angle-ply laminates that are significantly affected by fiber scissoring. The compression strength for a $[90]_{48}$ laminate is used for the maximum matrix compression stress for the laminate, and this value is 255 MPa.

Specimens, Apparatus, and Tests

The 26 graphite-epoxy composite specimens tested in this investigation were fabricated from commercially available unidirectional Hercules AS4 graphite fiber tapes preimpregnated with 450-K cure Hercules 3502 thermosetting epoxy resin. The tapes were laid to form 48-ply laminates approximately 0.64 cm thick. The laminates were cured in an autoclave using the manufacturer's recommended procedure. Following cure, the laminates were ultrasonically C-scanned to establish specimen quality and then cut into test specimens. All specimens were 4.45 cm long and 3.81 cm wide. The loaded ends of each specimen were machined flat and parallel to

permit uniform compressive loading. The laminate stacking sequences are listed in Table 2. Two specimens for each laminate stacking sequence were tested.

Test specimens were loaded to failure in axial compression using a 1.33-MN-capacity hydraulic testing machine. The loaded ends of the specimen were clamped by fixtures during testing, and a typical specimen with the support fixture is shown in Fig. 6. The specimens were tested to failure by slowly applying a compressive load to simulate a static loading condition.

The test specimens and fixtures used in this study are simple and compact. This specimen and fixture have been used successfully for material characterization tests[17] and were selected for this study because of their simplicity. Some compression test methods for composite laminates use specimens with short test sections (e.g., 1.27 cm[18]) or require elaborate fixtures that completely support the test specimen along the length.[19] These methods may inhibit the natural failure mode for a laminate.

Table 2 Young's modulus and failure data for compression-loaded laminates

Stacking sequence	Young's modulus, GPa	Failure stress, MPa	Failure strain, %
$[0]_{48}$	130.9	958.0	1.09[a]
$[0]_{48}$	134.3	932.4	0.98
$[\pm 5/\mp 5]_{6s}$	129.0	910.2	1.08
$[\pm 5/\mp 5]_{6s}$	129.6	946.9	1.14
$[\pm 10/\mp 10]_{6s}$	119.3	883.9	1.05
$[\pm 10/\mp 10]_{6s}$	124.9	801.1	0.91
$[\pm 15/\mp 15]_{6s}$	102.4	636.8	0.79
$[\pm 15/\mp 15]_{6s}$	103.5	603.2	0.76
$[\pm 20/\mp 20]_{6s}$	88.3	431.7	0.65
$[\pm 20/\mp 20]_{6s}$	85.0	361.1	0.46
$[\pm 30/\mp 30]_{6s}$	45.9	245.0	0.50
$[\pm 30/\mp 30]_{6s}$	45.0	201.2	0.44
$[\pm 45/\mp 45]_{6s}$	16.5	177.1	1.59
$[\pm 45/\mp 45]_{6s}$	18.4	178.6	1.74
$[\pm 60/\mp 60]_{6s}$	12.0	271.9	4.93
$[\pm 60/\mp 60]_{6s}$	12.1	266.6	4.67
$[\pm 70/\mp 70]_{6s}$	11.0	255.1	3.37
$[\pm 70/\mp 70]_{6s}$	10.8	270.9	3.87
$[\pm 75/\mp 75]_{6s}$	10.1	239.6	3.08
$[\pm 75/\mp 75]_{6s}$	9.7	253.8	3.53
$[\pm 80/\mp 80]_{6s}$	10.2	237.9	3.09
$[\pm 80/\mp 80]_{6s}$	10.3	249.7	3.05
$[\pm 85/\mp 85]_{6s}$	10.5	230.1	2.73
$[\pm 85/\mp 85]_{6s}$	10.6	225.5	2.56
$[90]_{48}$	10.3	249.5	2.90
$[90]_{48}$	10.1	260.5	3.19

[a]Failure strain calculated using laminate end shortening and original length rather than from strain gauge.

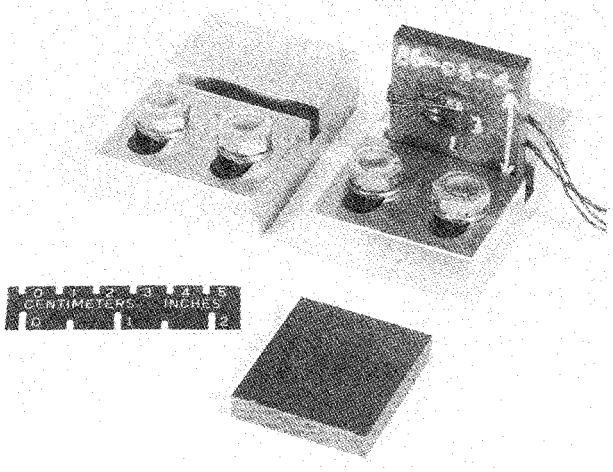

Fig. 6 Compressive test specimen and fixture.

The present compression test method uses a specimen that is sized to be thick enough to avoid global buckling and to be both long and wide enough to minimize boundary condition effects. The present method also uses a simple test fixture that introduces load without overly supporting the specimen.

Electrical resistance strain gages were used to monitor strains and direct current differential transformers were used to monitor longitudinal displacement of the ends. The location on the specimen of the back-to-back axial and transverse strain gages is shown in Fig. 6. Electrical signals from the instrumentation and the corresponding applied loads were recorded on magnetic tape at regular time intervals during the test.

Results and Discussion

The experimental and analytical results for this study are described in this section. Experimental results include stress-strain curves and tabulated data. Young's modulus, failure stress, and failure strain data are given in Table 2. Failure data for all laminates except the $[\pm 45/\mp 45]_{6s}$ laminates correspond to a catastrophic event that terminates the load-carrying capability of the laminate. Failure data for the $[\pm 45/\mp 45]_{6s}$ laminates correspond to the near-zero slope of the stress-strain curve. The failure strain is calculated using laminate end shortening because the failure strain for some laminates exceeded the capability of the strain gages. Stress-strain data for specimens having similar failure modes are presented together, and these failure modes are described. The experimental results are compared to predictions for failure stress and failure mode.

Experimental Results

Typical stress-strain data for $[0]_{48}$, $[\pm 5/\mp 5]_{6s}$, and $[\pm 10/\mp 10]_{6s}$ specimens are shown in Fig. 7. These data are nearly

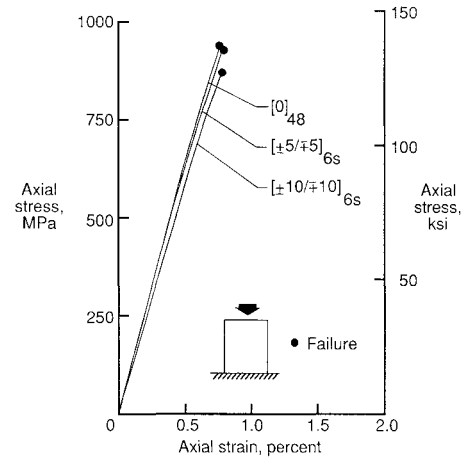

Fig. 7 Axial stress-strain response for typical laminates that fail by interlaminar shearing.

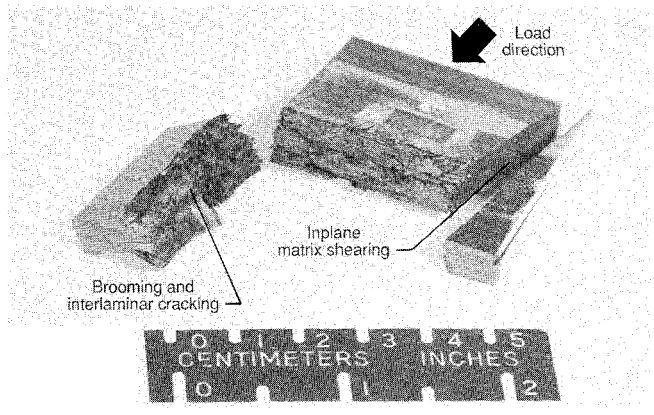

Fig. 8 Failed $[\pm 10/\mp 10]_{6s}$ laminate.

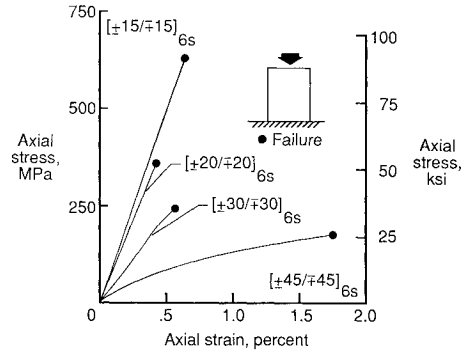

Fig. 9 Axial stress-strain response for typical laminates that fail by in-plane matrix shearing.

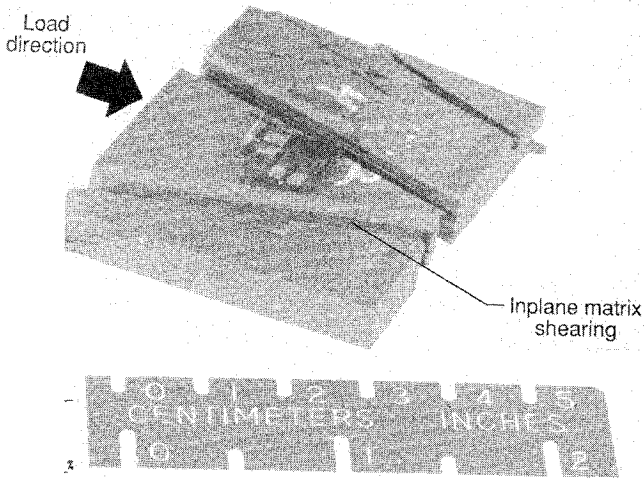

Fig. 10 Failed [± 15/ ∓ 15]$_{6s}$ laminate.

linear to failure, and these specimens have the highest strengths of all specimens tested. The dominant failure mode for this group of specimens is interlaminar shearing. This failure mode is illustrated in Fig. 8. The interlaminar shearing failure mode is characterized by brooming and interlaminar cracking.

Typical stress-strain data for [± 15/ ∓ 15]$_{6s}$, [± 20/ ∓ 20]$_{6s}$, [± 30/ ∓ 30]$_{6s}$, and [± 45/ ∓ 45]$_{6s}$ specimens are shown in Fig. 9. The degree of nonlinearity for these data increases with increasing fiber angle, and the strength for the laminates in this group spans a wide range. The dominant failure mode for this group of specimens is in-plane matrix shearing (see Fig. 10). In-plane matrix shearing in angle-ply laminates is characterized by failure surfaces that are parallel to the fiber direction as shown in the figure. A dramatic change in a laminate's dominant failure mode is shown by comparing Figs. 8 and 10. The dominant mode changes from interlaminar shearing to in-plane matrix shearing for only a 5-deg change in fiber orientation. Coupling between the interlaminar shearing mode and the in-plane matrix shearing mode is indicated by the presence of these two failure modes in the failed [± 10/ ∓ 10]$_{6s}$ laminate in Fig. 8.

Typical stress-strain data for [± 60/ ∓ 60]$_{6s}$, [± 70/ ∓ 70]$_{6s}$, [± 75/ ∓ 75]$_{6s}$, [± 80/ ∓ 80]$_{6s}$, [± 85/ ∓ 85]$_{6s}$, and [90]$_{48}$ specimens are shown in Figs. 11a and 11b. The data are very nonlinear, and these specimens have the highest failure strains for all specimens tested. The square symbols on the figure correspond to data recorded immediately before exceeding the strain-gage capability. Laminate failure stress and strain are greater than the respective data corresponding to the square symbols. All the strength results for the laminates in this group are approximately equal. The dominant failure mode for this group of specimens is matrix compression (see Fig. 12). The matrix compression failure mode is characterized by a failure

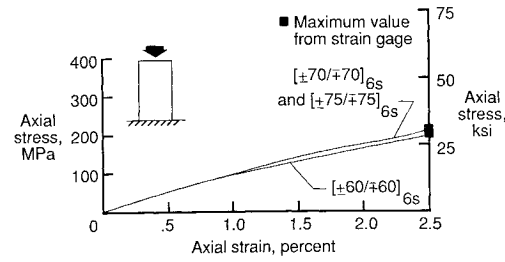

a) Results for [± 60/ ∓ 60]$_{6s}$, [± 70/ ∓ 70]$_{6s}$, and [± 75/ ∓ 75]$_{6s}$ laminates

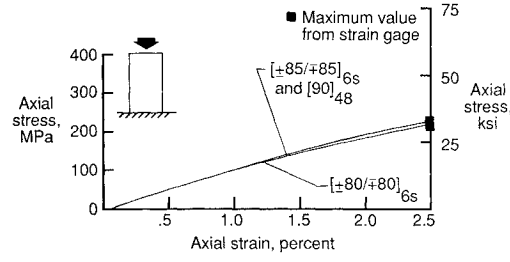

b) Results for [± 80/ ∓ 80]$_{6s}$, [± 85/ ∓ 85]$_{6s}$, and [90]$_{48}$ laminates

Fig. 11 Axial stress-strain response for typical laminates that fail by matrix compression.

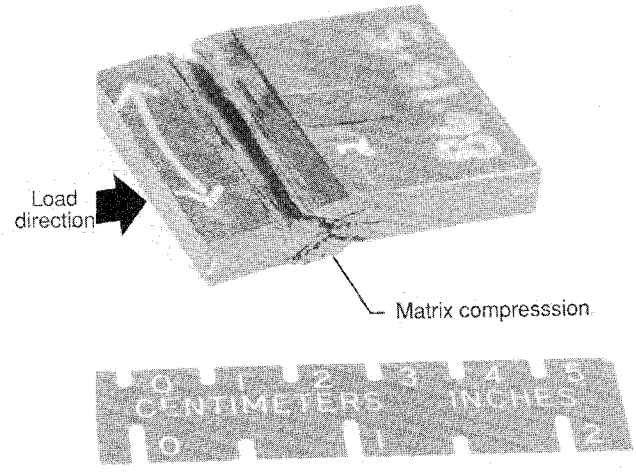

Fig. 12 Failed [90]$_{48}$ laminate.

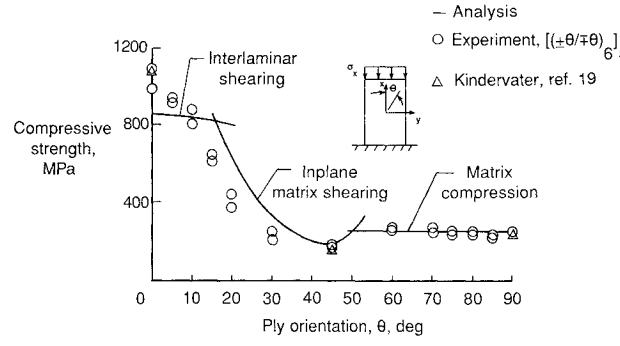

Fig. 13 Compressive strength as a function of ply orientation for [± θ]$_s$-class AS4/3502 laminates.

surface that extends through the laminate thickness and is oriented at 45 deg to the middle surface.

Comparison of Analytical and Experimental Results

Laminate compressive strength as a function of ply orientation is shown in Fig. 13 for [± θ]$_s$-class AS4/3502 laminates. The laminate compressive strength is dominated by the three

failure mechanisms mentioned previously: interlaminar shearing, in-plane matrix shearing, and matrix compression. The stress associated with each failure mechanism is calculated, and the lowest or critical stress is the predicted laminate compressive strength. This strength is plotted as a solid line on the figure. The analysis predicts that interlaminar shearing initiates laminate failure for $0 \le \theta \le 15$ deg, in-plane matrix shearing initiates laminate failure for $15 \le \theta \le 50$ deg, and matrix compression initiates laminate failure for $50 \le \theta \le 90$ deg. Experimental results are plotted as symbols on the figure. The analytical and experimental results from the present study show good agreement for $\theta < 45$ deg and show excellent agreement for $\theta \ge 45$ deg. Similar experimental results for AS4/3502 laminates[20] are also plotted on the figure and also agree with the analytical results.

Fiber scissoring is an important mechanism for the $[\pm\theta]_s$-class laminates when $50 \le \theta < 90$ deg. Fiber scissoring causes the initial fiber angle to increase, thereby both decreasing the load carried by the fibers and increasing the load carried by the matrix for a given applied load. The analysis indicates that the fiber-scissoring mechanism does not significantly affect the behavior of the $[\pm\theta]_s$-class laminates in this study for $0 \le \theta < 50$ deg. The analysis also indicates that the fiber-scissoring mechanism does significantly affect the behavior of the $[\pm\theta]_s$-class laminates in this study for $50 \le \theta < 90$ deg. The result of the load redistribution caused by fiber scissoring for laminates with $50 \le \theta < 90$ deg is to decrease the in-plane shearing stress parallel to the fiber and to increase the compressive stress in the matrix. The amount of fiber scissoring in these laminates is sufficient to change the predicted dominant failure mechanism from in-plane matrix shearing (as suggested in Ref. 18 for $50 \le \theta \le 75$ deg) to matrix compression. The dominance of the matrix compression failure mode is characteristic of laminates significantly affected by fiber scissoring. The response of such laminates approaches the response of a $[90]_{48}$ laminate as the fiber angle increases, and the matrix is the primary load-carrying constituent for $[90]_{48}$ laminates. The experimental results agree very well with the predicted matrix compression failure mode.

Concluding Remarks

This paper describes the failure of selected compression-loaded multidirectional composite laminates. A general nonlinear theory is presented for predicting laminate failure. The theory includes the effects of laminate initial imperfections, such as out-of-plane waviness and in-plane waviness of fibers. The theory also includes the effects of fiber scissoring in angle-ply laminates. The theory identifies interlaminar shearing, in-plane matrix shearing, and matrix compression as dominant failure mechanisms for compression-loaded $[\pm\theta]_s$-class laminates. Experimental results for the $[\pm\theta]_s$-class laminates are presented and include failure stress, failure strain, and laminate failure modes. A simple compressive test technique is described.

The general nonlinear theory predicts the compressive failure modes and strengths for the $[\pm\theta]_s$-class laminates in this study. Interlaminar shearing is shown to be the dominant failure mode for $0 \le \theta \le 15$ deg. In-plane matrix shearing is shown to be the dominant failure mode for $15 \le \theta \le 50$ deg. Matrix compression is shown to be the dominant failure mode for $50 \le \theta \le 90$ deg. The analytical and experimental strength data show good agreement for $\theta < 45$ deg and show excellent agreement for $\theta \ge 45$ deg.

References

[1]Dow, N. F. and Gruntfest, I. J., "Determination of Most-Needed, Potentially Possible Improvements in Materials for Ballistic and Space Vehicles," General Electric Co., Philadelphia, PA, Air Force Contract AF 04 (647)-269, T.I.S. R60SD389, June 1960.

[2]Rosen, B. W., "Mechanics of Composite Strengthening," *Fiber Composite Materials,* American Society for Metals, Metals Park, OH, 1965, pp. 37–75.

[3]Greszczuk, L. B., "Microbuckling of Unidirectional Composites," U. S. Air Force, Wright-Patterson AFB, OH, AFML-TR-71-231, Jan. 1972.

[4]Greszczuk, L. B., "Failure Mechanics of Composites Subjected to Compressive Loading," U.S. Air Force, Wright-Patterson AFB, OH, AFML-TR-72-107, Aug. 1972.

[5]Evans, A. G. and Adler, W. F., "Kinking as a Mode of Structural Degradation in Carbon Fiber Composites," *Acta Metallurgica,* Vol. 26, May 1978, pp. 725–738.

[6]Maewal, A., "Postbuckling Behavior of Periodically Laminated Medium in Compression," *International Journal of Solids and Structures,* Vol. 17, No. 3, March 1981, pp. 335–344.

[7]Budiansky, B., "Micromechanics," *Computers and Structures,* Vol. 16, No. 1-4, Jan. pp. 3–12.

[8]Hahn, H. T. and Williams, J. G., "Compression Failure Mechanisms in Unidirectional Composites," NASA TM 85834, August 1984.

[9]Suarez, J. A., Whiteside, J. B., and Hadcock, R. N., "The Influence of Local Failure Modes on the Compressive Strength of Boron/Epoxy Composites," *Composite Materials: Testing and Design (Second Conference), ASTM STP 497,* American Society for Testing and Materials, Philadelphia, PA, 1972, pp. 237–256.

[10]Rotem, A. and Hashin, Z., "Failure Modes for Angle Ply Laminates," *Journal of Composite Materials,* Vol. 9, April 1975, pp. 191–206.

[11]Kim, R. Y., "On the Off-Axis and Angle-Ply Strength of Composites," *Test Methods and Design Allowables for Fibrous Composites, ASTM STP 734,* edited by C. C. Chamis, American Society for Testing and Materials, Philadelphia, PA, pp. 91–108.

[12]Shuart, M. J., "Short-Wavelength Buckling and Shear Failures for Compression-Loaded Composite Laminates," Ph.D. Dissertation, Univ. of Delaware, Newark, Dec. 1985; also available as NASA TM 87640, Nov. 1985.

[13]Zimmerman, R. S., Adams, D. F., and Walrath, D. E., "Investigation of the Relations Between Neat Resins and Advanced Composite Mechanical Properties, Volume I—Results," NASA CR-172303, Nov. 1984.

[14]Koiter, W. T., "On the Stability of Elastic Equilibrium," Ph.D. Dissertation, Delft, H. J. Paris, Amsterdam, 1945. English translation, Air Force Flight Dynamics Laboratory, Wright-Patterson AFB, OH, AFFDL-TR-70-25, Feb. 1970.

[15]Shuart, M. J. and Williams, J. G., "Compression Behavior of $\pm 45°$-Dominated Laminates with a Circular Hole or Impact Damage," *AIAA Journal,* Vol. 24, Jan. 1986, pp. 115–122.

[16]Rosen, B. W., "A Simple Procedure for Experimental Determination of the Longitudinal Shear Modulus of Unidirectional Composites," *Journal of Composite Materials,* Vol. 6, Oct. 1972, pp. 552–554.

[17]Dexter, H. B. and Funk, J. G., "Impact Resistance and Interlaminar Fracture Toughness of Through-the-Thickness Reinforced Graphite/Epoxy," AIAA Paper 86-1020, May 1986.

[18]"D 3410-75 Standard Test Method for Compressive Properties of Unidirectional or Crossply Fiber-Resin Composites,," *1982 Annual Book of ASTM Standards, Part 36,* American Society for Testing and Materials, Philadelphia, PA, 1982, pp. 872–880.

[19]Sandorff, P. E., Ryder, J. T., and Lauraitis, K. N., "Experimental Evaluation of Column Compression Properties of Graphite/Epoxy Composites," *Composites Technology Review,* Vol. 3, No. 1, Spring 1981, pp. 6–16.

[20]Kindervarter, Ch., "Compression and Crush Energy Absorption Behavior of Composite Laminates," *Proceedings of the E/MRS Conference on Advanced Materials Research and Development for Transport,* DFVLR, Stuttgart, FRG, Nov. 1985, pp. 1–9.